

## Modeling surface processes and kinetics of compound layer formation during plasma nitriding of pure iron

F. León Cázares<sup>a</sup>, A. Jiménez Cenicerros<sup>a</sup>, J. Oseguera Peña<sup>a,b</sup>, and F. Castillo Aranguren<sup>a,b,\*</sup>

<sup>a</sup>Instituto Tecnológico y de Estudios Superiores de Monterrey, Campus Estado de México, Carretera al Lago de Guadalupe Km 3.5, Atizapán de Zaragoza, Estado de México, 52926, México.

<sup>b</sup>Trames S.A. de C.V., Calle Bohemia 11 5, Cuautitlán Izcalli, Estado de México, 54766, México.

\*e-mail: francast@itesm.mx

Received 5 November 2013; accepted 25 March 2014

Different approaches have been developed concerning growth description of the compact nitride layers, especially those produced by ammonia. Nitriding by plasma uses a glow discharge technology to introduce nitrogen to the surface which in turn diffuses itself into the material. During this process, the ion bombardment causes sputtering of the specimen surface.

This paper presents a mathematical model of compound layer formation during plasma nitriding of pure iron. The model takes into account the erosion effect at the plasma-solid interface due to sputtering. This erosion effect is computer simulated and adjusted in order to consider its contribution to the study of layer growth kinetics. The model is presented as a moving boundary diffusion problem, which considers the observed qualitative behavior of the process.

**Keywords:** Diffusion; plasma nitriding; layer growth kinetics; sputtering.

PACS: 81.65-b; 68.35.Fx; 66.30.je

### 1. Introduction

Thermochemical nitriding treatments in several varieties of steel are widely used in industry because of their broad application range [1,2]. Nitriding can be performed with gases containing ammonia [3-5] or with cyanide salts [6], as well as by weakly ionized plasmas [1,2,7]. The nitrogen flow from the surface to the bulk material leads to allotropic transformations that notably enhance the mechanical and chemical properties of the workpiece. The combination of a compact layer of nitrides, followed by a nitrogen diffusion zone in ferrite, results in an improved wear resistance, a significant increase in hardness from the surface towards the interior of the part, and in many cases in an improvement of fatigue resistance. In general, interaction with other surfaces lead to a decrease in friction coefficients, as well as to an improved corrosion resistance [1,2]. Plasma assisted thermochemical treatments allow diffusion to occur at low temperatures compared to other processes, so that very low distortions are developed in the pieces. Additionally, these treatments produce no pollutants [1,2,7].

Several authors have modeled the concomitant growth of compact layers of nitrides in the Fe-N thermodynamic system [8-23]. Concerning gas nitriding, taking into consideration the important role of the nitrogen potential, and thus its surface concentration, descriptions of the concomitant growth of the layers have been carried out as a quasi-steady state regime. In different models the displacement of the interfaces is assumed to be parabolic for the whole process. However, based on the moving boundary mathematical approximation it is not necessary to assume *a priori* a parabolic regime [24-27].

At the surface of the workpiece, grain boundaries, dislocations, and the orientation between the grains strongly affect the nitrogen transport in the solid at the beginning of the process. The formation of compact nitride layers highly depends on the defective configuration at the vicinity of the surface. Besides, a relevant aspect in the case of plasma nitriding is the surface sputtering. Some authors have considered the effects of this phenomenon in the analysis of the compact layers growth [28,29].

Considering a mass balance in each interface, taking into account a complete model of the sputtering process from the very beginning of the thermochemical treatment, whose relevance is particularly important in ferrite, based both on software simulations and experimental data, and without assuming neither a parabolic growth nor another specific behavior *a priori*, we have modeled the concomitant growth of compact nitride layers, as well as the nitrogen concentration profile at each phase, during ion nitriding in pure iron. The above mentioned elements provide a novel approach to the study of the compound layer formation.

### 2. Statement of the problem

#### 2.1. Surface erosion

In order to accurately develop the present model it is necessary to previously determine the sputtering rate. However, it cannot be assumed to be constant during the whole process due to the surface evolution. Many parameters should be taken into account to describe exactly this phenomenon such as plasma characteristics, surface roughness evolution and phase transitions in which iron nitrides are formed [28],

among others. This is the reason why it would be inappropriate to compare this model with experiments reported in literature [27] in which the conditions are not fully reported.

For practical purposes, an approximation based on different regimes is carried out taking into consideration the qualitative description of the process given in the pertinent literature [27-29].

It is possible to determine the sputtering rate for the first instants of the plasma nitriding process with the help of the *Stopping and Range of Ions in Matter* (SRIM) software [29] by running a specific simulation with the ion-energy distribution function of the given plasma. However, this analysis was specifically developed for pure iron. The sputtering rate decreases as the nitrogen surface concentration increases, so that once the nitride layer is formed and it has grown to a thickness higher than the maximum ion implantation depth in the bulk material, a steady-state regime lower than the initial rate is reached due to the allotropic transformation. This rate is modeled, for a transition period of time, through a fourth degree polynomial to ensure that its profile is continuous and smooth. The final value for this erosion rate was extracted from literature [27] concerning similar nitriding processes.

## 2.2. Mathematical model

The following mathematical model describes the layer growth kinetics and nitrogen profile concentration at each phase and diffusion zone during ion nitriding of pure iron. The model represents a moving boundary value problem. There has been an ongoing effort on the simulation of layer growth kinetics and nitrogen concentration profiles in ion nitriding during the last decades [27,30-32]. These research papers have yielded interesting results. However, usually,

severe conditions are imposed on the kinetics of the growth process. Meanwhile, consistency and interrelationship of the process data have not often been considered. These kinds of restrictions have frequently diminished the accuracy and significance of the obtained results.

The present model takes into account surface erosion [27,30-32] and its effect on the problem in a slightly different way. Moreover, in the mathematical setting of the problem, the evolution of the diffusion zone is characterized through a fictitious moving boundary. Both elements are introduced in order to obtain a more accurate approach to the description of the original problem.

The proposed model studies ion nitriding of pure iron once the compound layer is already formed. This takes place just after the incubation period and before the settlement of the quasi-steady state of the layer growth. Hence, the plasma nitriding process of pure iron is studied right after the incubation of phases  $\epsilon$  and  $\gamma'$ . The growth of the concomitant layers and the interfaces is characterized as a phenomenon through Fick's Second Law, mass balance at the interfaces, and the corresponding solubility limits of each layer.

In building the mathematical model of the problem the following assumptions are made:

- The surface erosion and layer growth occur in plane fronts parallel to the specimen surface.
- Evolution of phases takes place under thermodynamical equilibrium conditions.
- Mass balance at the interfaces considers equal specific volumes.
- Flow is one-dimensional.

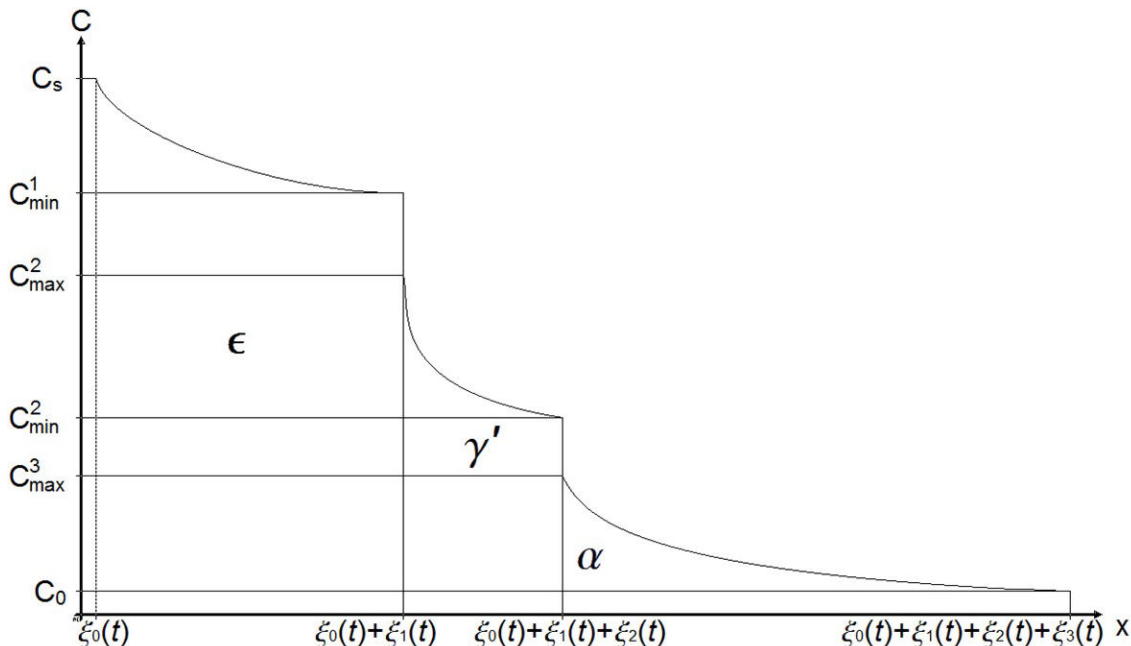


FIGURE 1. Nitrogen concentration profiles, layers, interfaces and plasma-metal boundary in iron at 803.15 K.

- Diffusion coefficients are constant at each phase and diffusion zone.
- The temperature at every point in the specimen is identical during the whole process.

Notice that in the present article there is no *a priori* assumption on the parabolic layer growth.

Let  $t_0$  be the time from which layers  $\varepsilon$ ,  $\gamma'$  and diffusion zone  $\alpha$  are assumed to be formed and begin to evolve. Let us denote by  $\xi_0(t)$  the displacement of the surface in time  $t > t_0$  respect to its original position  $x = 0$  for  $t = 0$ ; and  $\xi_1(t)$  represents the  $\varepsilon$ -layer thickness for  $t > t_0$ . Let  $\xi_2(t)$  be the thickness of the  $\gamma'$ -layer for  $t > t_0$ . Also,  $\xi_3(t)$  symbolizes the thickness of the diffusion zone at time  $t > t_0$ , measured from the adjacent interface to a fictitious moving boundary which is determined by a null flux condition on it. Figure 1 illustrates the nitrogen concentration profiles, layers, diffusion zone and interfaces, including the plasma-solid one.

Then, the model has the following form

$$\frac{\partial C_1}{\partial t} = D_1 \frac{\partial^2 C_1}{\partial x^2}, \quad t > t_0, \quad \xi_0(t) < x < \xi_0(t) + \xi_1(t) \quad (1)$$

$$\frac{\partial C_2}{\partial t} = D_2 \frac{\partial^2 C_2}{\partial x^2}, \quad t > t_0, \quad \xi_0(t) + \xi_1(t) < x < \xi_0(t) + \xi_1(t) + \xi_2(t) \quad (2)$$

$$\frac{\partial C_3}{\partial t} = D_3 \frac{\partial^2 C_3}{\partial x^2}, \quad t > t_0, \quad \xi_0(t) + \xi_1(t) + \xi_2(t) < x < \xi_0(t) + \xi_1(t) + \xi_2(t) + \xi_3(t) \quad (3)$$

Moreover,

$$\xi_1'(t) = \frac{-D_1 \frac{\partial C_1}{\partial x} \Big|_{x=(\xi_0(t)+\xi_1(t))^-} + D_2 \frac{\partial C_2}{\partial x} \Big|_{x=(\xi_0(t)+\xi_1(t))^+}}{C_{\min}^1 - C_{\max}^2} - \xi_0'(t) \quad (7)$$

$$\xi_2'(t) = \frac{-D_2 \frac{\partial C_2}{\partial x} \Big|_{x=(\xi_0(t)+\xi_1(t)+\xi_2(t))^-} + D_3 \frac{\partial C_3}{\partial x} \Big|_{x=(\xi_0(t)+\xi_1(t)+\xi_2(t))^+}}{C_{\min}^2 - C_{\max}^3} - \xi_0'(t) - \xi_1'(t) \quad (8)$$

Where  $\xi_0'(t)$ ,  $\xi_1'(t)$ ,  $\xi_2'(t)$ ,  $\xi_3'(t)$  stand for the derivatives of  $\xi_0(t)$ ,  $\xi_1(t)$ ,  $\xi_2(t)$ ,  $\xi_3(t)$  respectively, represent the mass balance (Stefan condition) at each interface.

$$\frac{\partial C_3}{\partial x}(x, t) \Big|_{x=(\xi_0(t)+\xi_1(t)+\xi_2(t)+\xi_3(t))^-} = 0 \quad (9)$$

Describes the flux null condition at the fictitious moving boundary which divides the diffusion zone from the substrate. This contrasts with (7) and (8), which express the mass balance at the interfaces between the layers. It means that beyond this fictitious moving border there is no nitrogen diffusion.

Finally,

$$\xi_i(t_0) = x_i, \quad i = 1, 2, 3 \quad (10)$$

Where  $C_i = C_i(x, t)$ ,  $i = 1, 2, 3$  represent the nitrogen concentration at depth  $x$  for time  $t$  and  $D_i$ ,  $i = 1, 2, 3$  are the effective diffusion coefficients at each phase and diffusion zone. Then, (1)-(3) express the Fick's Second Law at each section.

$$C_i(x, t_0) = f(x), \quad i = 1, 2, 3 \quad (4)$$

Express the initial nitrogen concentration for the time  $t_0$ .

$$C_1(x, t) \Big|_{x=\xi_0(t)^+} = C_S \quad (5)$$

Represents the boundary condition on the surface.

$$C_1(x, t) \Big|_{x=(\xi_0(t)+\xi_1(t))^-} = C_{\min}^1 \quad (6a)$$

$$C_2(x, t) \Big|_{x=(\xi_0(t)+\xi_1(t))^+} = C_{\max}^2 \quad (6b)$$

Indicate the jump at the interface between  $\varepsilon$  and  $\gamma'$  with solubility limits  $C_{\min}^1$  and  $C_{\max}^2$ .

$$C_2(x, t) \Big|_{x=(\xi_0(t)+\xi_1(t)+\xi_2(t))^-} = C_{\min}^2 \quad (6c)$$

$$C_3(x, t) \Big|_{x=(\xi_0(t)+\xi_1(t)+\xi_2(t))^+} = C_{\max}^3 \quad (6d)$$

Represent the jump at the interface between  $\gamma'$  and  $\alpha$  with solubility limits  $C_{\min}^2$  and  $C_{\max}^3$ .

$$C_3(x, t) \Big|_{x=(\xi_0(t)+\xi_1(t)+\xi_2(t)+\xi_3(t))^-} = C_0 \quad (6e)$$

Stands for the nitrogen concentration at the fictitious moving boundary which separates the diffusion zone from the substrate.

Denote the thicknesses of layer and diffusion zone for time  $t_0$ .

Meanwhile, the separation  $\xi_0(t)$  from the original surface caused by the surface erosion is modeled through

$$\xi_0(t) = \begin{cases} \beta_1 t, & 0 \leq t \leq t_0 \\ a t^4 + b t^3 + c t^2 + d t + e, & t_0 \leq t \leq t_1 \\ \beta_2 t + f, & t_1 \leq t \end{cases} \quad (11)$$

$\beta_1$  denotes the sputtering rate obtained through the SRIM simulation for the ferritic phase and remains constant in  $[0, t_0]$ . This rate is assumed to be a decreasing function of

time in  $[t_0, t_1]$  until it becomes constant again from  $t_1$  on, at a sputtering rate  $\beta_2$ . The decreasing section of  $\xi_0(t)$  is modeled through a fourth order polynomial fit in  $[t_0, t_1]$ , which represents the behavior of the surface erosion. This fourth order polynomial enables a smooth transition of the surface displacement for the elapsing time between sputtering rates  $\beta_1$  and  $\beta_2$ .

### 3. Solution of the mathematical model

In such a way, the model (1)-(11) describes the layer and diffusion zone growth kinetics in the transient stage: layers are completely formed and evolve to a quasi-steady state following a moving boundary diffusion pattern in  $C_i(x, t)$ ,  $i = 1, 2, 3$ , where Stefan conditions are prescribed at the interfaces  $\xi_0(t) + \xi_1(t)$ ,  $\xi_0(t) + \xi_1(t) + \xi_2(t)$ . The solution to problem (1)-(11) is sought using Goodman's method (heat balance integral method HBIM [33-35]).

Concentration profiles  $C_i(x, t)$ ,  $i = 1, 2, 3$  are represented by

$$C_1(x, t) = C_{\min}^1 + a_1(t)(\xi_0(t) + \xi_1(t) - x) + b_1(t)(\xi_0(t) + \xi_1(t) - x)^2 \quad (12)$$

$$\xi_0(t) < x < \xi_0(t) + \xi_1(t), \quad t > t_0$$

$$C_2(x, t) = C_{\min}^2 + a_2(t)(\xi_0(t) + \xi_1(t) + \xi_2(t) - x) + b_2(t)(\xi_0(t) + \xi_1(t) + \xi_2(t) - x)^2 \quad (13)$$

$$\xi_0(t) + \xi_1(t) < x < \xi_0(t) + \xi_1(t) + \xi_2(t), \quad t > t_0$$

$$C_3(x, t) = C_{\max}^3 + a_3(t)(\xi_0(t) + \xi_1(t) + \xi_2(t) - x) + b_3(t)(\xi_0(t) + \xi_1(t) + \xi_2(t) - x)^2 \quad (14)$$

$$\xi_0(t) + \xi_1(t) + \xi_2(t) < x < \xi_0(t) + \xi_1(t) + \xi_2(t) + \xi_3(t), \quad t > t_0$$

It means  $C_i(x, t)$ ,  $i = 1, 2, 3$  are to be found as analytical approximate solutions to (1)-(11).

The unknowns are now  $a_i(t)$ ,  $b_i(t)$ ,  $\xi_i(t)$ ,  $i = 1, 2, 3$ . Note that statements (12)-(14) guarantee the fulfillment of the jump conditions (6a), (6c) and (6d) at the interfaces. Also, from the decreasing behavior of  $C_i(x, t)$ ,  $i = 1, 2, 3$  as functions of the space variable for fixed times and Fick's Second Law it follows that  $a_i(t) > 0$ ,  $b_i(t) > 0$   $i = 1, 2, 3$ .

Conditions (5), (6b) y (6d) become

$$C_{\min}^1 + a_1(t)\xi_1(t) + b_1(t)\xi_1^2(t) = C_S \quad (15)$$

$$C_{\min}^2 + a_2(t)\xi_2(t) + b_2(t)\xi_2^2(t) = C_{\max}^2 \quad (16)$$

$$C_{\max}^3 - a_3(t)\xi_3(t) + b_3(t)\xi_3^2(t) = C_0 \quad (17)$$

Null flux condition (9) takes the form

$$a_3(t) - 2b_3(t)\xi_3(t) = 0 \quad (18)$$

The use of Stefan conditions at each interface yield

$$\frac{a_1(t)}{C_{\min}^1 - C_{\max}^2} (D_1 a_1(t) - D_2 a_2(t) - 2D_2 b_2(t)\xi_2(t)) = 2D_1 b_1(t) \quad (19)$$

$$\frac{a_2(t)}{C_{\min}^2 - C_{\max}^3} (D_2 a_2(t) - D_3 a_3(t)) = 2D_2 b_2(t) \quad (20)$$

Mass balance integrals at each phase and diffusion zone produce the following three non-linear ODE in the same unknowns as the previous polynomials equations.

$$(C_S - C_{\min}^1) \xi_0'(t) + \left( \frac{1}{2} a_1'(t) + \frac{1}{3} b_1'(t) \xi_1(t) \right) \xi_1^2(t) + (a_1(t) + b_1(t) \xi_1(t)) \xi_1(t) \xi_1'(t) = 2D_1 b_1 \xi_1(t) \quad (21)$$

$$(C_{\max}^2 - C_{\min}^2) (\xi_0'(t) + \xi_1'(t)) + \left( \frac{1}{2} a_2'(t) + \frac{1}{3} b_2'(t) \xi_2(t) \right) \xi_2^2(t) + (a_2(t) + b_2(t) \xi_2(t)) \xi_2(t) \xi_2'(t) = 2D_2 b_2(t) \xi_2(t) \quad (22)$$

$$(C_{\max}^3 - C_0) (\xi_0'(t) + \xi_1'(t) + \xi_2'(t) + \xi_3'(t)) - \left( \frac{1}{2} a_3'(t) - \frac{1}{3} b_3'(t) \xi_3(t) \right) \xi_3^2(t) - (a_3(t) - b_3(t) \xi_3(t)) \xi_3(t) \xi_3'(t) = 2D_3 b_3(t) \xi_3(t) \quad (23)$$

Equations (15)-(23) form a system of differential-algebraic equations (DAE) in  $a_i(t)$ ,  $b_i(t)$ ,  $\xi_i(t)$ ,  $i = 1, 2, 3$ . A detailed deduction of this system is found in the Appendix. In solving the resulting DAE system, initial conditions for the unknown are to be prescribed. Initial conditions for  $\xi_i(t)$ ,  $i = 1, 2, 3$  could be obtained using experimental results, once the layers are already formed at time  $t_0$ . Meanwhile, initial conditions for the coefficients  $a_i(t)$ ,  $b_i(t)$ ,  $i = 1, 2, 3$  at time  $t_0$  could be found from the polynomial equations (15)-(20).

In such a way, the initial conditions found as indicated above, guarantee that the solutions (12)-(14) approximately satisfy the initial condition (4) of the original problem.

### 4. Numerical results and discussion

A strategy for solving the DAE system is to differentiate the polynomial equations (15) - (20) in order to get ordinary differential equations in the same unknowns. The new equations and the remaining three (21)-(23) form an ODE system subjected to the corresponding initial conditions, which is numerically solved.

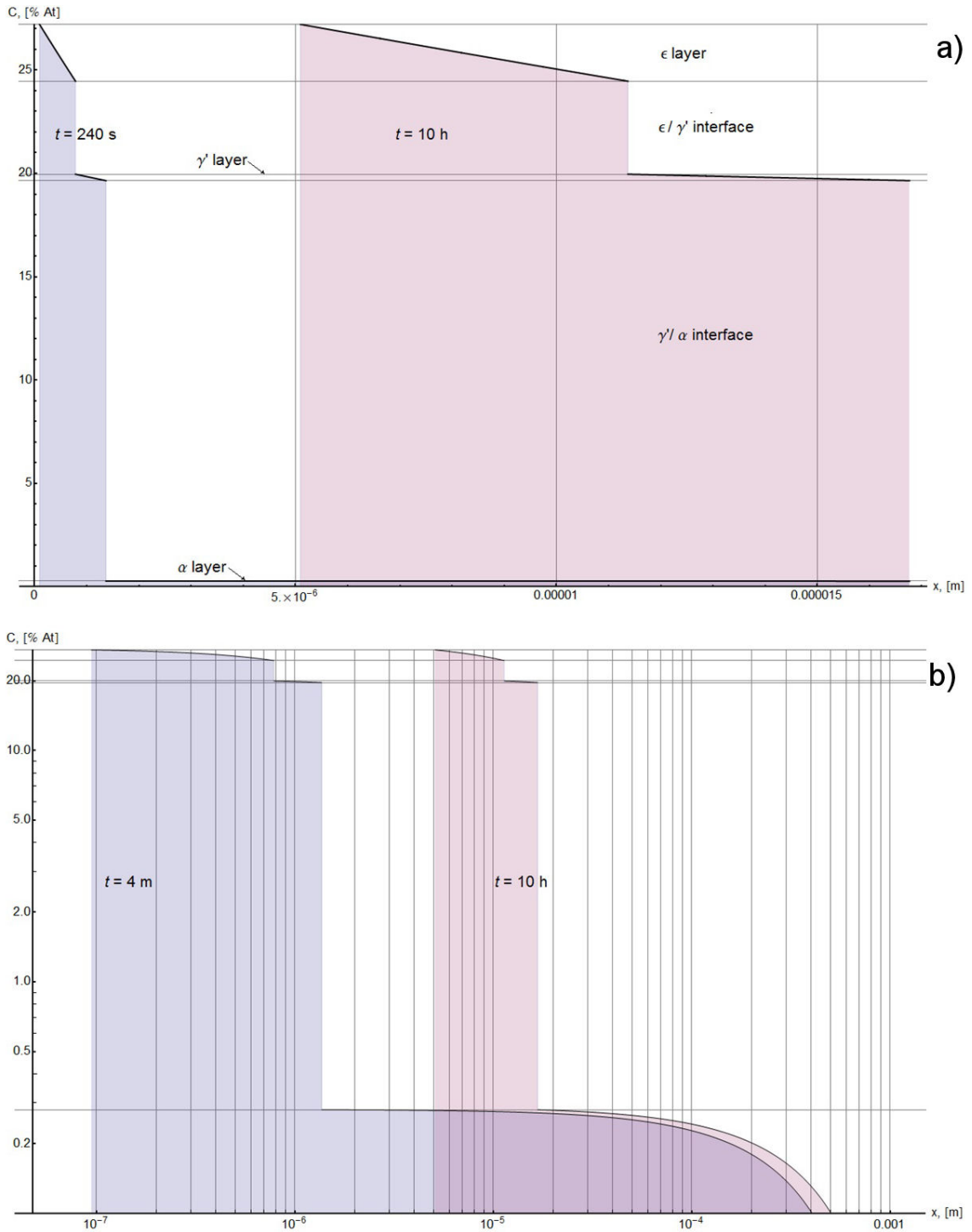


FIGURE 2. (a) Nitrogen concentration profiles for  $t = 240$  s and  $t = 36,000$  s. (b) Log-log plot of a), which provides a better view of the diffusion zone.

The experimental values of  $C_S$ ,  $C_{\max}^i$ ,  $C_{\min}^i$ ,  $D_i$ ,  $i = 1, 2, 3$  are taken from [36]:

$$C_S = 27.211 \text{ at. } \%, \quad C_{\min}^1 = 24.460 \text{ at. } \%, \\ C_{\max}^2 = 19.959 \text{ at. } \%, \quad C_{\min}^2 = 19.649 \text{ at. } \%, \\ C_{\max}^3 = 0.28 \text{ at. } \%,$$

$$C_0 = 0 \text{ at. } \%, \\ D_1 = 1.7385 \times 10^{-14} \text{ m}^2/\text{s}, \\ D_2 = 1.1525 \times 10^{-13} \text{ m}^2/\text{s}, \\ D_3 = 5.6646 \times 10^{-12} \text{ m}^2/\text{s}$$

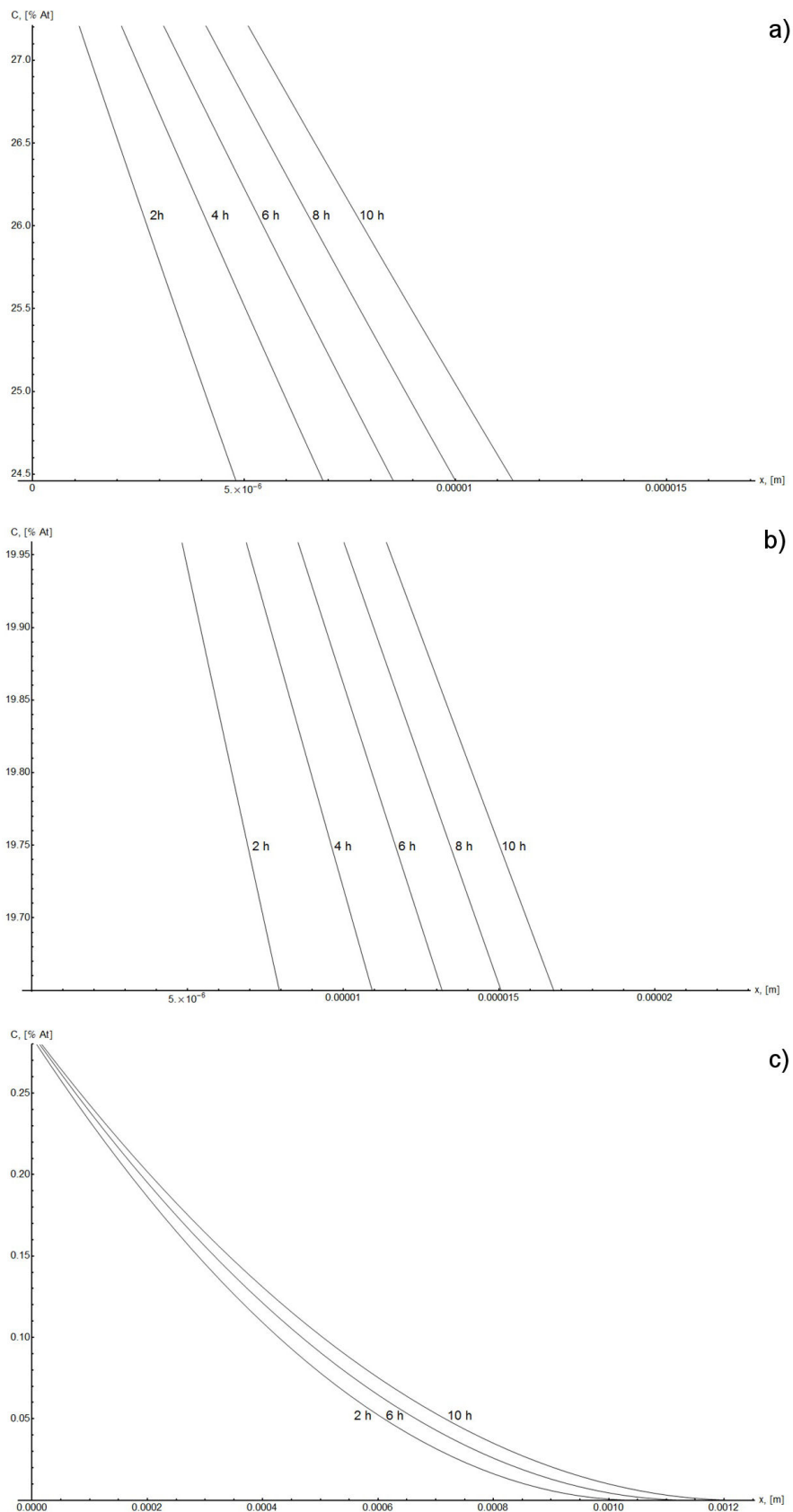


FIGURE 3. Nitrogen concentration profiles for each phase at different times. (a)  $\epsilon$  phase for  $t = 2, 4, 6, 8, 10$  h. (b)  $\gamma'$  phase for  $t = 2, 4, 6, 8, 10$  h. (c)  $\alpha$  phase for  $t = 2, 6, 10$  h..

Computer simulations allow to set

$$\begin{aligned}
 t_0 &= 120 \text{ s}, & \xi_1(120) &= 10^{-7} \text{ m}, \\
 \xi_2(120) &= 10^{-6} \text{ m}, & \xi_3(120) &= 10^{-3} \text{ m}, \\
 \beta_1 &= 3.998 \times 10^{-10} \text{ m/s} \\
 \beta_2 &= 1.3889 \times 10^{-10} \text{ m/s}
 \end{aligned}$$

The initial conditions are found to be:

$$\begin{aligned}
 a_1(120) &= 2.24347 \times 10^7, & a_2(120) &= 307773, \\
 a_3(120) &= 560 \\
 b_1(120) &= 5.07531 \times 10^{13}, & b_2(120) &= 2.22658 \times 10^9,
 \end{aligned}$$

$$b_3(120) = 280000$$

Computing was performed on a PC at 2.4 GHz using Mathematica version 8. The results of the numerical experiments yield:

- The numerical solution of the ODE system initial problem associated to equations (15)-(23) with the prescribed initial conditions.
- The behavior of the layer thicknesses and interfaces.
- The nitrogen concentration profiles at each phase and diffusion zone.
- Curve fitting of the layers and diffusion zone thicknesses.

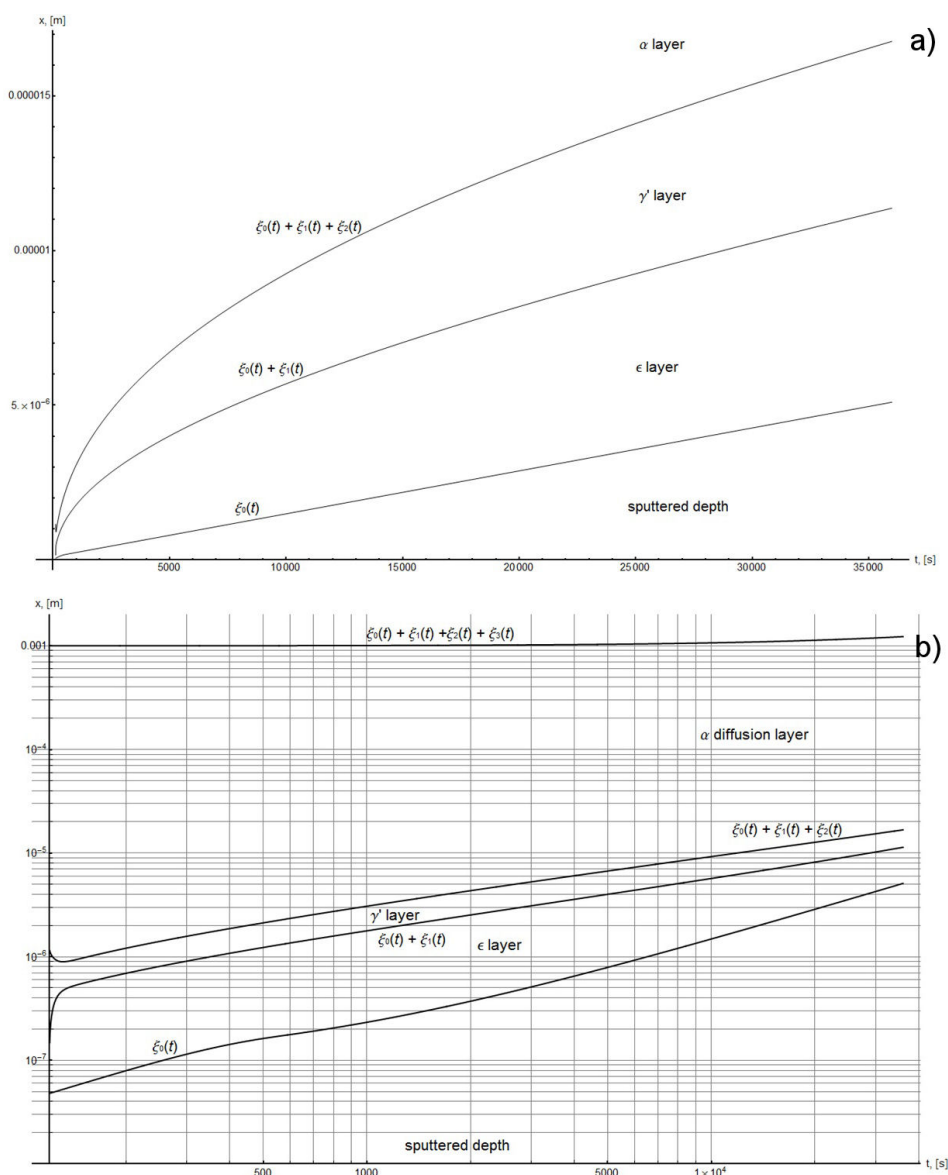


FIGURE 4. Evolution of the different interfaces depths. (a) Layer interfaces and sputtered depth. (b) Layer interfaces, fictitious boundary and the sputtered depth in a log-log plot.

Figure 2 shows the nitrogen concentration profiles in layers  $\varepsilon$ ,  $\gamma'$  and diffusion zone for the variable erosion regime proposed in this work. It is observed the expected behavior for different times according to reference data at 530°C. In Fig. 2b, log-log curves allow to appreciate the thickness of the diffusion zone.

In Fig. 3 the evolution of the concentration profiles is shown for each layer and diffusion zone at different times. The qualitative behavior of the concentration profiles is similar to the observed response for different nitriding regimes (with or without the sputtering phenomenon).

Figure 4 exhibits the erosion profile and its influence in the kinetics of the interfaces. From figure 4b it is significant to point out that the behavior of the fictitious boundary, which divides the diffusion zone from the substrate as introduced in the model following Goodman's method, is not parabolic.

Figure 5 shows the profiles of the compound layer thickness for different sputtering rate regimes: no erosion, Marciniak's constant, variable (proposed in this paper), and SRIM constant erosion rates. The thickness kinetics of the compound layer under variable erosion rate, as proposed in this work, is bounded by the thickness kinetics of the comp-

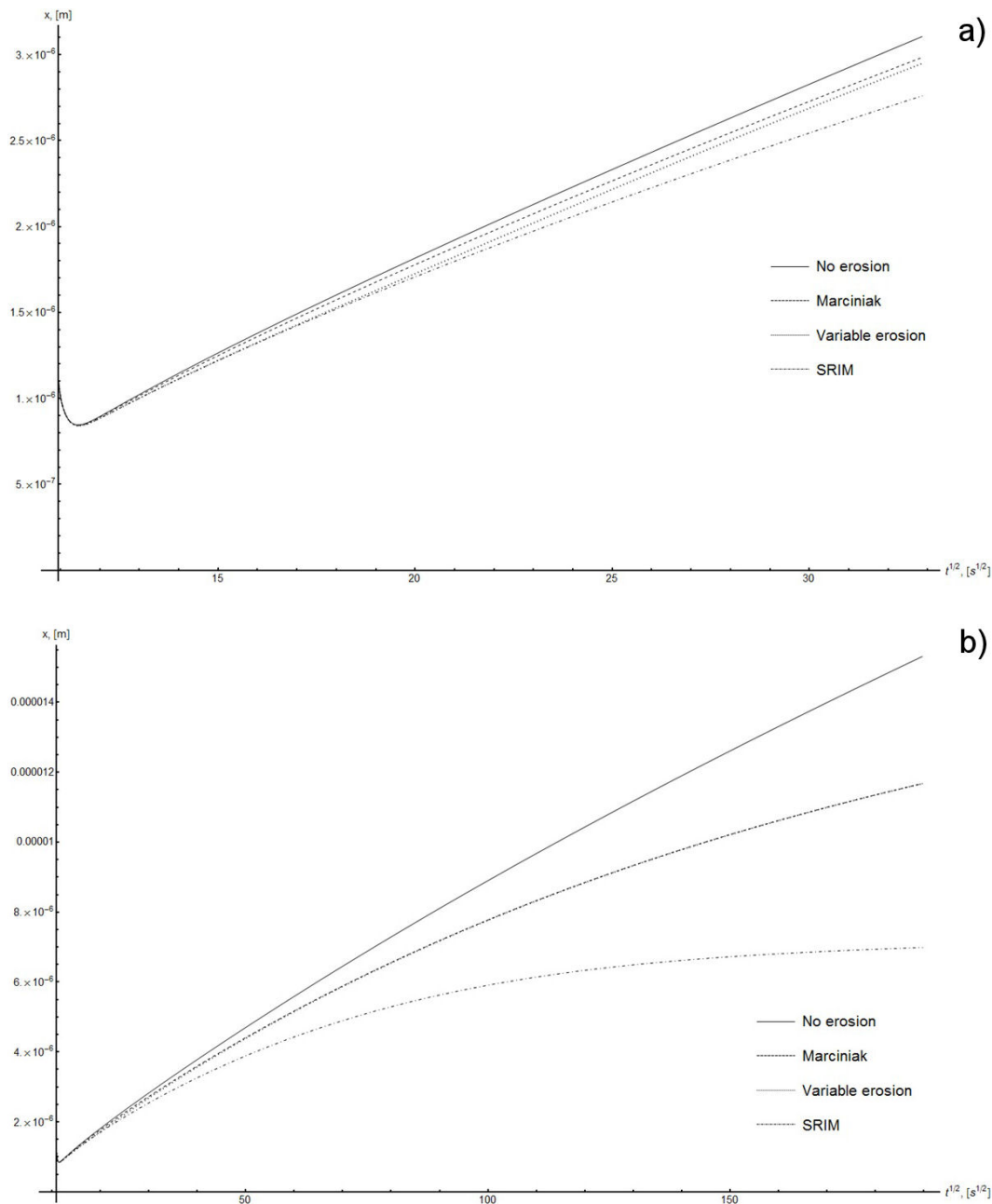


FIGURE 5. Evolution of the nitride compound layer thickness with different sputtering rate regimes: no erosion, Marciniak's constant, variable and SRIM's constant erosion rate for (a) short times and (b) large times.

ound layer modeled with constant erosion rates upon where the present model is built. As it can be seen, for long periods of time the variable sputtering rate effect becomes negligible as the compound layer thickness clearly approaches the Marciniak’s constant erosion profile. It is worth to mention that this figure exhibits that the compound layer thicknesses considering sputtering are significantly narrower than the one with no erosion. The noticed behavior is in full agreement with the conclusion of other authors [20].

### 5. Conclusions

The layer growth kinetics during plasma nitriding of pure iron could be studied considering different stages associated to the formation a coalescence of  $\gamma' - Fe_4 N_{1-x} y \varepsilon - Fe_2 N_{1-z}$  precipitates.

The present work addresses the description of the layer growth kinetics and nitrogen concentration profiles once the layers are formed, and evolve following a moving boundary pattern. The research presents

- A correctly stated mathematical model of the problem, which takes into account the surface erosion.
- The adequacy and consistency of the mathematical model with the mass transfer mechanism (Fick’s Second Law and mass-balance at the interfaces) and the relevant information of the problem (diffusion coefficients and nitrogen solubility limits).
- The study and solution of the mathematical model using Goodman’s method (heat balance integral method).
- The approximate analytical solutions are obtained without *a priori* assumptions on the layer growth, avoiding the use of pre-established solutions of the diffusion equations which are not directly related to the studied problem.
- The results of the present model qualitatively agree with the research of other authors [20,30-32]. Nevertheless, in the present work the modeling of the sputtering rate is based on a computer simulation of the ionic implantation through SRIM. This approach enriches the study of the layer kinetics during ion nitriding of pure iron.
- The curve fitting of the obtained layer growth exposes the qualitative behavior observed by other authors [20]: “initially the nitride layer grows rapidly, but the rate falls below the parabolic law after longer times”.

The consideration of the above mentioned elements provides a novel and original approach to the study of the compound layer formation and kinetics during plasma nitriding of pure iron. The obtained results allow further research, and qualitative and quantitative understanding of nitriding processes.

### Appendix

Next, a detailed deduction of (19)-(23) is presented. See also [24].

From condition 6a) it follows

$$\begin{aligned} & \frac{dC_1(x,t)}{dt} \Big|_{x=(\xi_0(t)+\xi_1(t))^-} \\ &= \frac{\partial C_1(x,t)}{\partial x} (\xi'_0(t) + \xi'_1(t)) \Big|_{x=(\xi_0(t)+\xi_1(t))^-} \\ &+ \frac{\partial C_1(x,t)}{\partial t} \Big|_{x=(\xi_0(t)+\xi_1(t))^-} = 0 \end{aligned}$$

Which yields

$$-a_1(t) (\xi'_0(t) + \xi'_1(t)) + 2D_1 b_1(t) = 0 \tag{A.1}$$

On the other hand, the mass balance condition (7) leads to

$$\begin{aligned} \xi'_1(t) &= \frac{1}{C_{min}^1 - C_{max}^2} \left[ D_1 a_1(t) \right. \\ &\left. - D_2 (a_2(t) + 2b_2 \xi_2(t)) \right] - \xi'_0(t) \tag{A.2} \end{aligned}$$

Combining (A1) with (A2) the algebraic Eq. (19) is obtained

$$\begin{aligned} & \frac{a_1(t)}{C_{min}^1 - C_{max}^2} (D_1 a_1(t) - D_2 a_2(t) \\ & - 2D_2 b_2(t) \xi_2(t)) = 2D_1 b_1(t) \tag{A.3} \end{aligned}$$

Analogously, from 6c) and mass balance condition (8), the algebraic Eq. (20) can be inferred

$$\frac{a_2(t)}{C_{min}^2 - C_{max}^3} (D_2 a_2(t) - D_3 a_3(t)) = 2D_2 b_2(t) \tag{A.4}$$

ODE (21)-(23) are deducted using mass balance integral along each phase and diffusion zone.

Then, Fick’s Second Law in phase  $\varepsilon$ , where  $\xi_0(t) < x < \xi_0(t) + \xi_1(t)$ , is accomplished in average as

$$\int_{\xi_0(t)}^{\xi_0(t)+\xi_1(t)} \frac{\partial C_1}{\partial t} dx = \int_{\xi_0(t)}^{\xi_0(t)+\xi_1(t)} D_1 \frac{\partial^2 C_1}{\partial x^2} dx \tag{A.5}$$

This mass balance integral can be calculated as follows.

$$\begin{aligned} & \int_{\xi_0(t)}^{\xi_0(t)+\xi_1(t)} \frac{\partial C_1}{\partial t} dx \\ &= \frac{d}{dt} \left( \int_{\xi_0(t)}^{\xi_0(t)+\xi_1(t)} C_1(x,t) dx \right) \\ & - C_{min}^1 (\xi'_0(t) + \xi'_1(t)) + C_S \xi'_0(t) \tag{A.6} \end{aligned}$$

Which, employing (12), turns into

$$\int_{\xi_0(t)}^{\xi_0(t)+\xi_1(t)} \frac{\partial C_1}{\partial t} dx = \left( \frac{a_1'(t)}{2} + \frac{b_1'(t)}{3} \xi_1(t) \right) \xi_1^2(t) + (a_1(t) + b_1(t)\xi_1(t)) \xi_1(t) \xi_1'(t) + (C_S - C_{\min}^1) \xi_0'(t) \quad (A.7)$$

Furthermore

$$\int_{\xi_0(t)}^{\xi_0(t)+\xi_1(t)} D_1 \frac{\partial^2 C_1}{\partial x^2} dx = D_1 \left[ \frac{\partial C_1(x, t)}{\partial x} \Big|_{x = (\xi_0(t)+\xi_1(t))} - \frac{\partial C_1(x, t)}{\partial x} \Big|_{x = \xi_0(t)} \right] \quad (A.8)$$

Again, thanks to (12), it leads to

$$\int_{\xi_0(t)}^{\xi_0(t)+\xi_1(t)} D_1 \frac{\partial^2 C_1}{\partial x^2} dx = D_1 [-a_1(t) + a_1(t) + 2b_1(t)\xi_1(t)] = 2D_1 b_1(t)\xi_1(t) \quad (A.9)$$

Combining (A7) with (A9) the referred ODE (21) is obtained

$$(C_S - C_{\min}^1) \xi_0'(t) + \left( \frac{1}{2} a_1'(t) + \frac{1}{3} b_1'(t) \xi_1(t) \right) \xi_1^2(t) + (a_1(t) + b_1(t) \xi_1(t)) \xi_1(t) \xi_1'(t) = 2D_1 b_1 \xi_1(t) \quad (A.10)$$

Fick's Second Law in phase  $\gamma'$ , where  $\xi_0(t) + \xi_1(t) < x < \xi_0(t) + \xi_1(t) + \xi_2(t)$ , in average yields

$$\int_{\xi_0(t)+\xi_1(t)}^{\xi_0(t)+\xi_1(t)+\xi_2(t)} \frac{\partial C_2}{\partial t} dx = \int_{\xi_0(t)+\xi_1(t)}^{\xi_0(t)+\xi_1(t)+\xi_2(t)} D_2 \frac{\partial^2 C_2}{\partial x^2} dx \quad (A.11)$$

Similarly

$$\int_{\xi_0(t)+\xi_1(t)}^{\xi_0(t)+\xi_1(t)+\xi_2(t)} \frac{\partial C_2}{\partial t} dx = \frac{d}{dt} \left[ \int_{\xi_0(t)+\xi_1(t)}^{\xi_0(t)+\xi_1(t)+\xi_2(t)} C_2(x, t) dx \right] - C_{\min}^2 (\xi_0'(t) + \xi_1'(t) + \xi_2'(t)) + C_{\max}^2 (\xi_0'(t) + \xi_1'(t)) \quad (A.12)$$

Now, thanks to expression  $C_2(x, t)$  in (13) it follows that

$$\int_{\xi_0(t)+\xi_1(t)}^{\xi_0(t)+\xi_1(t)+\xi_2(t)} \frac{\partial C_2}{\partial t} dx = \left( \frac{a_2'(t)}{2} + \frac{b_2'(t)}{3} \xi_2(t) \right) \xi_2^2(t) + (a_2(t) + b_2(t)\xi_2(t)) \xi_2(t) \xi_2'(t) + (C_{\max}^2 - C_{\min}^2) (\xi_0'(t) + \xi_1'(t)) \quad (A.13)$$

Moreover

$$\int_{\xi_0(t)+\xi_1(t)}^{\xi_0(t)+\xi_1(t)+\xi_2(t)} D_2 \frac{\partial^2 C_2}{\partial x^2} dx = D_2 \left[ \frac{\partial C_2(x, t)}{\partial x} \Big|_{x = (\xi_0(t)+\xi_1(t)+\xi_2(t))} - \frac{\partial C_2(x, t)}{\partial x} \Big|_{x = (\xi_0(t)+\xi_1(t))} \right] \quad (A.14)$$

Which can be rewritten, employing (13), as

$$\int_{\xi_0(t)+\xi_1(t)}^{\xi_0(t)+\xi_1(t)+\xi_2(t)} D_2 \frac{\partial^2 C_2}{\partial x^2} dx = D_2 [-a_2(t) + a_2(t) + 2b_2(t)\xi_2(t)] = 2D_2 b_2(t)\xi_2(t) \quad (A.15)$$

Now, the combination of (A13) y (A15) leads to ODE (22)

$$(C_{\max}^2 - C_{\min}^2) (\xi_0'(t) + \xi_1'(t)) + \left( \frac{1}{2} a_2'(t) + \frac{1}{3} b_2'(t)\xi_2(t) \right) \xi_2^2(t) + (a_2(t) + b_2(t)\xi_2(t)) \xi_2(t)\xi_2'(t) = 2D_2 b_2(t)\xi_2(t) \quad (A.16)$$

Finally at the diffusion zone, where  $\xi_0(t) + \xi_1(t) < x < \xi_0(t) + \xi_1(t) + \xi_2(t)$  the mass balance integral becomes

$$\int_{\xi_0(t)+\xi_1(t)+\xi_2(t)}^{\xi_0(t)+\xi_1(t)+\xi_2(t)+\xi_3(t)} \frac{\partial C_3}{\partial t} dx = \int_{\xi_0(t)+\xi_1(t)+\xi_2(t)}^{\xi_0(t)+\xi_1(t)+\xi_2(t)+\xi_3(t)} D_3 \frac{\partial^2 C_3}{\partial x^2} dx \tag{A.17}$$

Analogously

$$\int_{\xi_0(t)+\xi_1(t)+\xi_2(t)}^{\xi_0(t)+\xi_1(t)+\xi_2(t)+\xi_3(t)} \frac{\partial C_3}{\partial t} dx = \frac{d}{dt} \left[ \int_{\xi_0(t)+\xi_1(t)+\xi_2(t)}^{\xi_0(t)+\xi_1(t)+\xi_2(t)+\xi_3(t)} C_3(x, t) dx \right] - C_0 (\xi'_0(t) + \xi'_1(t) + \xi'_2(t) + \xi'_3(t)) + C_{\max}^2 (\xi'_0(t) + \xi'_1(t) + \xi'_2(t)) \tag{A.18}$$

And the expression (14) of  $C_3(x, t)$  produces

$$\int_{\xi_0(t)+\xi_1(t)+\xi_2(t)}^{\xi_0(t)+\xi_1(t)+\xi_2(t)+\xi_3(t)} \frac{\partial C_3}{\partial t} dx = \left( -\frac{a'_3(t)}{2} + \frac{b'_3(t)}{3} \xi_3(t) \right) \xi_3^2(t) + (-a_3(t) + b_3(t)\xi_3(t)) \xi_3(t) \xi'_3(t) + (C_{\max}^3 - C_0) (\xi'_0(t) + \xi'_1(t) + \xi'_2(t) + \xi'_3(t)) \tag{A.19}$$

On the other hand

$$\int_{\xi_0(t)+\xi_1(t)+\xi_2(t)}^{\xi_0(t)+\xi_1(t)+\xi_2(t)+\xi_3(t)} D_3 \frac{\partial^2 C_3}{\partial x^2} dx = D_3 \times \left[ \frac{\partial C_3(x, t)}{\partial x} \Big|_{x=(\xi_0(t)+\xi_1(t)+\xi_2(t)+\xi_3(t))} - \frac{\partial C_3(x, t)}{\partial x} \Big|_{x=(\xi_0(t)+\xi_1(t)+\xi_2(t))} \right]$$

And the use of (14) gives

$$\int_{\xi_0(t)+\xi_1(t)+\xi_2(t)}^{\xi_0(t)+\xi_1(t)+\xi_2(t)+\xi_3(t)} D_3 \frac{\partial^2 C_3}{\partial x^2} dx = D_3 [-a_3(t) + a_3(t) + 2b_3(t)\xi_3(t)] = 2D_3 b_3(t)\xi_3(t) \tag{A.20}$$

In the end, ODE (23) is obtained from (A19) y (A20)

$$(C_{\max}^3 - C_0) (\xi'_0(t) + \xi'_1(t) + \xi'_2(t) + \xi'_3(t)) - \left( \frac{1}{2} a'_3(t) - \frac{1}{3} b'_3(t)\xi_3(t) \right) \xi_3^2(t) - (a_3(t) - b_3(t)\xi_3(t)) \xi_3(t)\xi'_3(t) = 2D_3 b_3(t)\xi_3(t) \tag{A.21}$$

<ol style="list-style-type: none"> <li>1. D. Pye, <i>Practical Nitriding and Ferritic Nitrocarburizing</i> (ASM International Materials Park, OH, 2003), pp. 204-7586.</li> <li>2. T. Bell et al., <i>Controlled Nitriding in Ammonia-Hydrogen Mixtures</i>, Source Book on Nitriding (American Society for Metals, 1977), pp. 259-265.</li> <li>3. M. O'Brien, <i>ASM Handbook</i>, <b>4</b>, (ASM International, OH, 1994), pp. 420.</li> <li>4. L. Torchane, P. Bilger, J. Dulcy and M. Gantois, <i>Metall. Mater. Trans. A</i> <b>27A</b> (1996) 1823.</li> <li>5. H. Du, <i>Gaseous Nitriding and Nitrocarburizing– Thermody-</i></li> </ol>	<ol style="list-style-type: none"> <li><i>namics and Kinetics.</i> (Thesis of Royal Institute of Technology, Stockholm, 1994).</li> <li>6. D. Gerardin, H. Michel and M.Gantois, <i>Scripta Metallurgica</i> <b>11</b> (1977) 557.</li> <li>7. G.E. Totten, <i>Steel Heat Treatment: Metalurgy and Technologies 2<sup>nd</sup> ed.</i> (CRC Press, Boca Raton, FL, 2004).</li> <li>8. M.A.J. Somers and E.J.Mittemeijer, <i>Surface Engineering</i> <b>3</b> (1987) 123.</li> <li>9. H.Du, <i>Journal of Phase Equilibria</i> <b>14</b> (1993) 682.</li> <li>10. H. Du, and J. Agren, <i>Metall Mater. Trans. A.</i> <b>27A</b> (1996) 1073.</li> </ol>
---	---

11. T. Christiansen and M.A.J. Somers, *Metall. Mater. Trans. A* **37A** (2006) 675.
12. E.J. Mittemeijer and M.A.J. Somers, *Surface Engineering* **13** (1997) 483.
13. B.J. Kooi, M.A.J. Somers and E.J. Mittemeijer, *Metallurgical and Materials Transactions A* **27A** (1996) 1055.
14. B.J. Kooi, M.A.J. Somers and E.J. Mittemeijer, *Metallurgical and Materials Transactions A* **27A** (1996) 1063.
15. M.A.J. Somers and E.J. Mittemeijer, *Metallurgical and Materials Transactions A* **26A** (1995) 57.
16. S.R. Hosseini, F. Ashrafizadeh, A. Kermanpur, *Iranian Journal of Science and Technology, Transaction B: Engineering* **34** (2010) 553.
17. Y.M. Lakhtin and Y.D. Kogan, *Nitriding of Steel* (Ed. Mashinostroenie, Moscow, 1976).
18. J.D. Fast and M.B. Verrijp, *Journal of the Iron and Steel Institute* **180** (1955) 337.
19. A. Ricard, J. Oseguera, L. Falk, H. Michel, and M. Gantois, *IEEE Trans. Plasma Sci.* **18** (1990) 940.
20. M.A.J. Somers and T. Christiansen, *J. of Phase Equilib. Diffus.* **26** (2005) 520.
21. T. Christiansen, and M.A.J. Somers, *Metall. Mater. Trans. A*, **37A** (2006) 675.
22. C. Jaoul, T. Belmonte, T. Czerwiec, D. Ablitzer, A. Ricard and H. Michel, *Thin Solid Films*, **506–507** (2006) 163.
23. T. Christiansen, K.V Dahl and M.A.J. Somers, M.A. J., *Mater.Sci. Technol.* **24** (2008) 159.
24. J. Bernal-Ponce, A. Fraguera-Collar., J. Oseguera-Peña and F.Castillo-Aranguren, *Proceedings of the 5th International Conference on Inverse Problems in Engineering: Theory and Practice* (Ed. Leeds University Press, Cambridge, 2005) B05.
25. F. Castillo, J. Oseguera, A. Fraguera, and A. Gómez, A., *Surf. Coat.Technol.* **203** (2008) 876.
26. A. Fraguera, F. Castillo, and J. Oseguera, *Rev. Mex. Fis.*, **56** (2010) 363.
27. A. Marciniak, *Surface Engineering* **1** (1985) 283.
28. R. Behrisch, *Topics in Applied Physics* **47** (Ed. Springer-Verlag, Berlin, 1981) pp. 4.
29. J. F. Ziegler, J. P. Biersack and U. Littmarck, *The Stopping and Ranges of Ion in Matter* (Ed. Pergamon Press, NY, 1985).
30. V. I. Dimitrov, J.D. Haen, G. Knuuyt, C. Quasyhaegens, L.M. Stals, *Appl. Phys.* **A63** (1996) 475.
31. V. I. Dimitrov, J.D. Haen, G. Knuuyt, C. Quasyhaegens, L.M. Stals, *Surface and Coatings Technology* **99** (1998) 234.
32. V. I. Dimitrov, G. Knuuyt, L.M. Stals, J.D. Haen, C. Quasyhaegens, *Appl. Phys.* **A67** (1998) 183.
33. T.R. Goodman, *Adv. Heat Transfer* **1** (1964) 51.
34. J. Crank, *Free and moving boundary problems.* (Ed. Clarendon Press, Oxford, 1987).
35. S. L. Mitchell, T.G. Myers, *International Journal of Differential Equations*, **2012**, (2012) Article ID 187902, <http://dx.doi.org/10.1155/2012/187902>
36. M. Gantois and J. Dulcy, *Theories des traitements thermochimiques- Nitruration- Nitrocarburation- Systemes binaire et ternaire fer-azote et fer azote-carbone. Couche de combinaison*, PACK: TRAITEMENT DES METAUX M 1224 (Ed. T.I., France, 2010) pp. 2-26